Supersonic Airplane Design Optimization Method for Aerodynamic Performance and Low Sonic Boom

Samson H. Cheung*
and
Thomas A. Edwards**

NASA Ames Research Center
Moffett Field, CA 94035

ABSTRACT

This paper presents a new methodology for the optimization of supersonic airplane designs to meet the dual design objectives of low sonic boom and high aerodynamic performance. Two sets of design parameters are used on an existing High Speed Civil Transport (HSCT) configuration to maximize the aerodynamic performance and minimize the sonic boom under the flight track. One set of the parameters perturbs the camber line of the wing sections to maximize the lift-over-drag ratio (L/D). A preliminary optimization run yielded a 3.75% improvement in L/D over a baseline low-boom configuration. The other set of parameters modifies the fuselage area to achieve a target F-function. Starting from an initial configuration with strong bow, wing, and tail shocks, a modified design with a flat-top signature is obtained. The methods presented can easily incorporate other design variables and objective functions. Extensions to the present capability in progress are described.

INTRODUCTION

The sonic boom element of NASA's High Speed Research Program includes low-boom aircraft design studies, atmospheric propagation research, and bioacoustic response studies. NASA Ames Research

*Research Scientist, MCAT Institute.
** Assistant Branch Chief, RFA.

Center has been investigating the use of computational fluid dynamics (CFD) to predict and design low-boom aircraft. Initially, validation studies were carried out that established the numerical requirements for accurate sonic boom predictions using CFD. Since then, attention has turned to the prospect of using CFD in the low-boom design process.

The need for simultaneous sonic boom and aerodynamic optimization was highlighted recently when it became clear that airplanes designed to a strict sonic boom constraint suffer an unacceptable performance penalty. A new proposed route structure for HSCT's incorporating supersonic corridors over land has relaxed the sonic boom constraint somewhat. On the other hand, reducing an airframer's market risk for a low-boom airplane necessitates that its aerodynamic performance nearly match that of a conventional design. Therefore, low-boom design studies must carefully balance the tradeoff between sonic boom loudness and aerodynamic performance.

Because of its generality, CFD offers the designer the opportunity to address many design issues simultaneously. An added advantage is that the geometry definition and performance data are common to any analysis or optimization problem. This paper demonstrates how the same computational tools can be used to optimize both sonic boom and aerodynamic efficiency. The theory and implementation of these techniques are briefly reviewed, then the optimization capability is exercised using a recently-developed low-boom configuration as an initial design (Ref. 1).

Several computational tools interconnect in the optimization procedure to be described. The CFD flow solver is the 3-D parabolized Navier-Stokes code UPS3D (Ref. 2). Although the code is capable of producing viscous flow results, it has been shown previously (Ref. 3) that inviscid analysis is sufficient for accurate sonic boom prediction. All results in this paper are based on the Euler equations for inviscid flow. The UPS3D code is supported by a hyperbolic grid generation scheme (Ref. 4) that is sufficiently fast and robust to operate within an automated optimization environment. The nonlinear optimizer NPSOL is based on a sequential quadratic programming algorithm in which the search direction is the solution of a quadratic programming subproblem (Ref. 5). The near-field pressure signal created by the airplane is extrapolated to the ground-level sonic boom by a routine based on Whitham's F-function and the equal-area rule (Refs. 6, 7). Finally, the perceived loudness (PLdB) of the sonic boom can be determined by Stevens' Mark VII method which involves Fast Fourier Transform on the energy spectrum of the sonic boom (Ref. 8).

AERODYNAMIC OPTIMIZATION

The Boeing low-boom model 1080-911 (Ref. 1) is used as the baseline configuration for the aerodynamic optimization studies. This configuration is 330 ft. long and is designed to cruise at Mach 1.7 at an altitude of 44,000 ft . A schematic of this configuration is shown in Fig. 1. The objective function to be maximized in this case is the lift-to-drag ratio, and the design parameters influenced the camber line of the wing sections. First, fine-grid CFD solutions were performed over a range of angles of attack to characterize the aerodynamics of this baseline configuration. These solutions indicated a maximum *L/D* of 18.23 at 4.0 degrees angle of attack.

Using CFD as an analysis tool for aerodynamic optimization requires that the inherent numerical errors of the solution are either negligibly small, or independent of the design perturbations. One means to insure this is to use very fine grids, which is computationally expensive. Another approach is to perform the optimization on a moderately coarse grid and then verify the end result with a fine-grid computation. This approach helps define the grid density for which the numerical errors are independent of the design perturbations. While the numerical value of *L/D* differs on coarse and fine grids, the increment due to design changes will be preserved when the errors on the coarse grid become independent of the design variables. In the present work, it was found that marching grid dimensions of 40 circumferential points by 30 radial points was not fine enough to produce reliable optimization trends, whereas further resolving the surface with a 67 by 30 grid produced consistent results on successively finer grids.

Design Optimization Parameters

Given a set of design parameters and the relevant constraints, the optimizer (NPSOL) will perturb the parameters and find the steepest gradient to search for the local minimum of the objective function. A widely used approach to aerodynamic optimization of an HSCT-type configuration is the use of shape functions (sine and exponential bumps) which are added in the airfoil sections (cf. Ref. 9). A difficulty with this approach is that the location and nature of the shape functions must be chosen carefully for each problem, and the values chosen for a particular configuration and flight condition may not be appropriate for a different case.

In this study, control points are defined on the camber line of each airfoil section as shown in Fig. 2. If y_i is the y-coordinate of the i^{th} control point, and δ_i is one of the design parameters, the new location of that control point is

$$y_i^{new} = y_i^{old} + T_{max}\,\delta_i$$

where T_{max} is the maximum thickness of the airfoil. The new airfoil is formed by splining through the control points with the thickness held fixed. For relatively straight camber lines, the control points are evenly distributed along the chord, whereas curved camber lines are defined by clustering control points in regions of curvature.

Results

For aerodynamic optimization, the lift-to-drag ratio was chosen as the objective function and the design parameters are control points along the camber line of each airfoil section. The wing is defined by twenty-six spanwise stations as shown in Fig. 3. To reduce the design space for this problem, two sets of five design parameters are used. The first set defines the camber line used for span stations 3 through 8 in the high-sweep region. The second set defines the camber line for stations 9 through 26. The five control points are evenly distributed along the camber line in both cases. The optimization run for this demonstration required approximately eighty flow solutions totaling four hours of Cray-YMP CPU time to give an optimized wing-body configuration with an L/D of 18.75 versus the original value of 18.03. Figure 4 compares the pressure on the lower surface of the original and optimized wing. Most of the increase in L/D results from a reduction of the wave drag, evidenced by the lower pressure on the wing leading edge. Figure 5 compares the airfoil section 3 of the original and optimized wing. A polar plot of L/D versus α for both the original and redesigned configurations is shown in Fig. 6. The L/D is uniformly higher for the optimized wing, and the maximum L/D is nearly 4% greater than the original geometry. It is interesting to note that there are only minor changes in the lift distribution and volume, so the aerodynamic optimization has a negligible effect on the sonic boom signature.

LINEAR SUPERSONIC THEORY

The low-boom design process in this paper makes use of linear supersonic theory which is widely used to predict the sonic boom of slender wing-body configurations (Refs. 10 and 11). For the sake of completeness, this method is briefly discussed.

Given a wing-body configuration, the equivalent area distribution due to volume, or A-function, can be easily determined by finding the area of the cross-section made by the cutting planes normal to the streamwise axis (x-axis). On the other hand, the equivalent area distribution due to lift, or B-function, is calculated by

$$B(x) = \frac{\beta}{2} \int_0^x C_p \, d\xi \tag{1}$$

where $\beta = \sqrt{M_\infty^2 - 1}$. In this paper, the B-function is calculated from the lift distribution predicted by the CFD code.

The total equivalent area distribution, $Ae(x)$, is the sum of $A(x)$ and $B(x)$. Then the F-function can be calculated by the Lighthill integral

$$F(y) = \frac{1}{2\pi} \int_0^\infty \sqrt{\frac{2}{\beta R(t)}} \, h\left(\frac{y-t}{\beta R(t)}\right) \, dAe'(t) \tag{2}$$

where $R(t) = \sqrt{Ae(t)/\pi}$, $Ae'(t)$ is the derivative of $Ae(t)$, and function h is

$$h(z) = \sqrt{\frac{\pi}{2p}} \frac{1}{K_1(p)} H(z)$$

In these expressions K_1 is the modified Bessel function of the second kind, p is Heaviside's operator of differentiation and $H(z)$ is the Heaviside unit step function. When extrapolated to a distance r_1, the F-function is shifted by the factor of $-\kappa\sqrt{r_1}F$, where $\kappa = (\gamma+1)(2\beta^3)^{-1/2} M_\infty^4$. This shifted F-function is muti-valued, so the location of the shock waves in the signature is determined by applying the equal-area rule. The pressure signal at distance r_1 is obtained by

$$\frac{\Delta p}{p_\infty} = \gamma M_\infty^2 F(y) / \sqrt{2\beta r_1} \tag{3}$$

$$x = y + \beta r_1$$

It should be noted that, by using the Abel transform, the equivalent area distribution can be found in term of F-function

$$Ae(x) \approx 4 \int_0^x \sqrt{x-t}\ F(t)\ dt \tag{4}$$

This form is particularly useful in the sonic boom minimization method to be described next.

SONIC BOOM MINIMIZATION

The sonic boom minimization method applied here is inspired by the method of Darden (Ref. 12), but uses CFD to provide an accurate description of the lift distribution and near-field pressure signal. First, a baseline flow solution is obtained and the ground-level sonic boom signature is determined by extrapolating the near-field pressure as described in Ref. 3. The equivalent area distribution for the configuration is generated as described above. The next step uses the optimizer to generate an equivalent area distribution with improved sonic boom characteristics. This is done by using the nine F-function parameters in Ref. 12 as "design" variables (see Fig. 7). The objective function in this case is a weighted combination of the sonic boom loudness (PLdB) and the deviation from the original area distribution:

$$\text{Objective Function} = (w_1 * \text{PLdB} + w_2 * D)/2. \tag{5}$$

where D is the deviation in L2 norm of the equivalent area distribution from the original design:

$$D = \| Ae - Ae(\text{original}) \|_2$$

and w_1 and w_2 are two weighting factors in the order of .001 and 1, respectively. Because the configuration used for this demonstration was designed for a flat-top signature, the F-function parameters were further constrained to achieve this result. Once the target F-function is defined, the new equivalent area is found using Eq. 4. In the present case, the equivalent area increments are applied only to the A-function. As a result, the lift distribution remains essentially unchanged and further CFD computations are not needed. In the future, the increments will be distributed between the A-function and B-function, necessitating flow solutions to generate the new equivalent area distribution.

The ground-level sonic boom of the original wing-body configuration at 4 degrees angle of attack is shown in Fig. 8. This result was obtained by extrapolating the flow solution from a distance of 1.25 body lengths to 133 body lengths. A strong intermediate shock is evident in the signature. However, the computational model did not include the nacelle geometry, and their effect on the far-field signature is under investigation. Figure 9 shows the equivalent area distribution of the original geometry using CFD for the lift distribution. The optimization routine developed a new area distribution based on a flat-top signature and minimal deviation from the original geometry, which is also shown in the figure. Note that, except for a small area near the nose, the new distribution adds equivalent area to the configuration.

Figure 10 compares the geometry of the original and modified configurations. The nose is visibly sharper, and the fuselage is somewhat larger in radius near the wing leading edge. Figure 11 compares the ground-level sonic boom for the two configurations. The modified configuration more nearly achieves the targeted flat-top signature. However, the perceived loudness was reduced by just 1 PLdB because the front shock was not allowed to change in this case. The lift-to-drag ratio increased by less than 1% as a result of these changes.

SUMMARY

Analysis and optimization computer codes have been joined to address design issues for an HSCT. Using CFD for aerodynamic analysis provides the accuracy and generality to study many different problems with the same basic methodology. The present work has demonstrated the ability to optimize aerodynamic efficiency and sonic boom loudness with a few simple design parameters. Applying this capability to a baseline low-boom configuration produced a 4% improvement in lift-to-drag ratio and eliminated an intermediate shock in a flat-top sonic boom signature with a small reduction in the loudness.

FUTURE WORK

The design capability described in this paper will be advanced along two lines in the near future. First, the design capability will be generalized somewhat. As mentioned earlier, equivalent area increments

for optimization will be applied to both volume and lift distributions for increased flexibility in design. By monitoring the aerodynamic performance as the lift distribution is manipulated, the dual design objectives may be optimized simultaneously. Second, development of a new low-boom configuration will be pursued using the complete geometry (including nacelles and empennage) of an existing low-boom geometry. The goal of this effort will be to advance the performance of a low-boom HSCT in terms of sonic boom loudness and lift-to-drag ratio as far as current technology permits.

REFERENCES

1. Haglund, George: Two HSCT Mach 1.7 Low Sonic Boom Designs. Invitational High-Speed Research Program Sonic Boom Workshop, NASA CP-3173, 1992.

2. Lawrence, S., Chaussee, D., and Tannehill, J.: Application of an Upwind Algorithm to the 3-D Parabolized Navier-Stokes Equations. AIAA Paper 87-1112, 1987.

3. Cheung, S., Edwards, T., and Lawrence, S.: Application of CFD to Sonic Boom Near and Mid Flow-Field Prediction. AIAA Paper 90-3999, 1990.

4. Chan, W., and Steger, J.: A Generalized Scheme for Three-Dimension Hyperbolic Grid Generator. AiAA Paper 91-1588, 1991.

5. Gill, P., Murray, W., Saunders, M., and Wright, M.: User's Guide for NPSOL, Technical Report SOL 86-2, Stanford University, CA 94305, 1986.

6. Whitham, G. B.: The flow Pattern of a Supersonic Projectile. Comm. Pure & Appl. Math., Vol. V, No. 3, 1952.

7. Lighthill, M. J.: Higher Approximation. General Theory of High Speed Aerodynamics, Vol. VI of High Speed Aerodynamics and Propulsion, Princeton University Press, 1954.

8. Stevens, S. S.: Perceived Level of Noise by Mark VII and Decibels (E). Jour. Acoust. Soc. Am., Vol. 51(2), 1972.

9. Chang, I. C., Torres, F., and van Dam, C.: Wing Design Code using 3-D Euler Equations and Optimization. AIAA Paper 91-3190, 1991.

10. Walkden, F.: The Shock Pattern of a Wing-Body Combination, Far from the Flight Path. Aeronaut. Q., Vol. IX, 1958

11. Gottlieb, J., and Ritzel, D.: Analytical Study of Sonic Boom From Supersonic Projectiles. Prog. Symposium, 1989.

12. Darden, Christine: Sonic Boom Minimization with Nose-Bluntness Relaxation. NASA Technical Paper 1348, 1979.

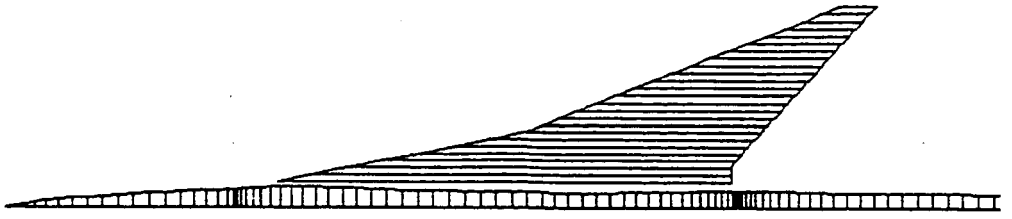

Figure 1. The wing-body configuration of the Boeing's 1080-911.

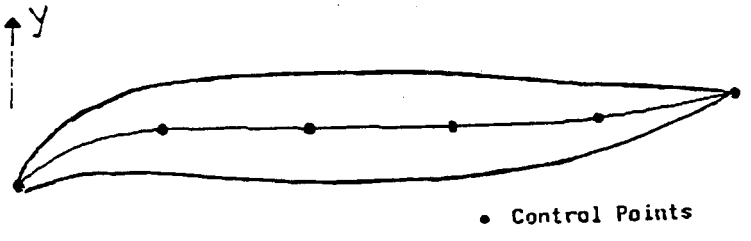

Figure 2. Control points on the camber line of a wing section.

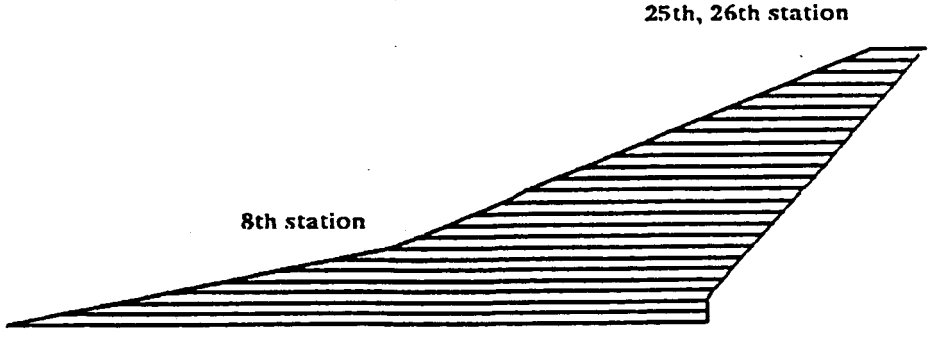

Figure 3. The spanwise wing sections of the Boeing's low-boom configuration.

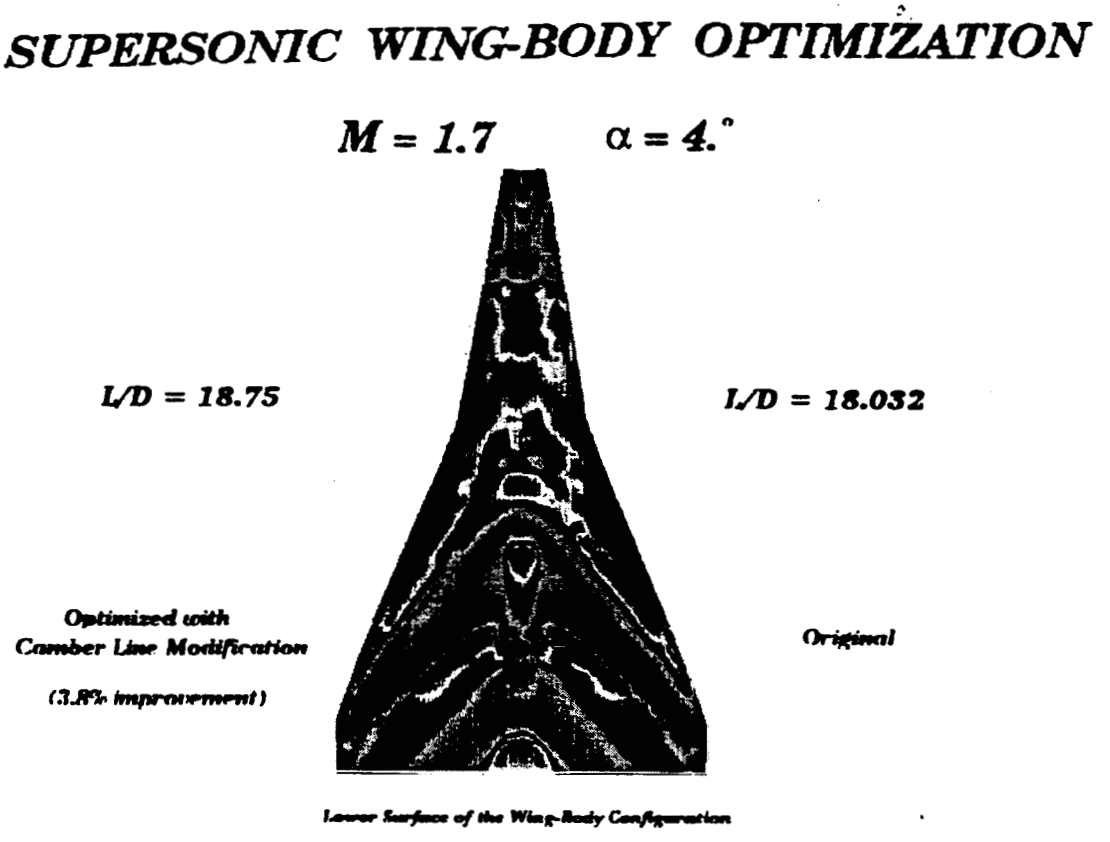

Figure 4. Pressure contour on the lower surfaces of the original and modified configuration.

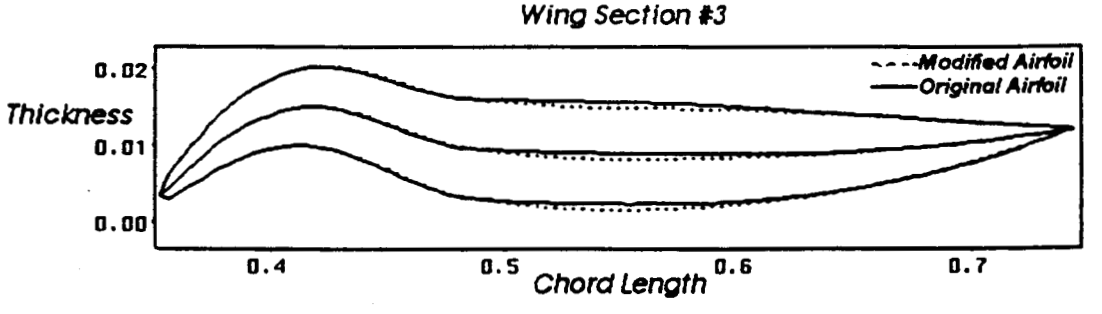

Figure 5. Airfoil section 3 of the original and optimized wing.

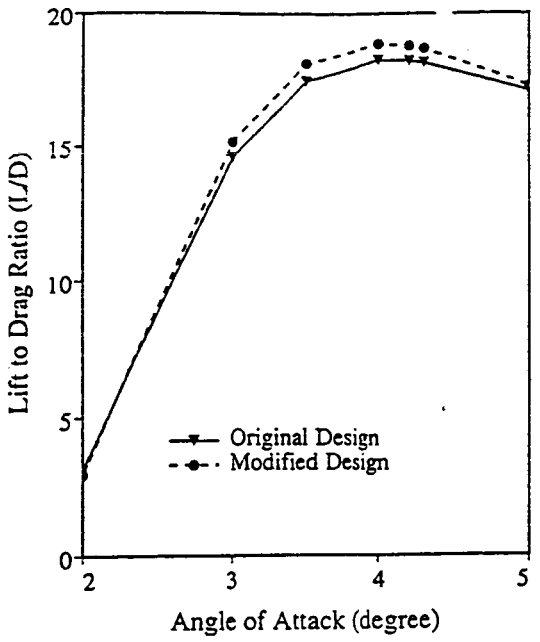

Figure 6. Polar plot of *L/D* versus α for the original and redesigned configurations.

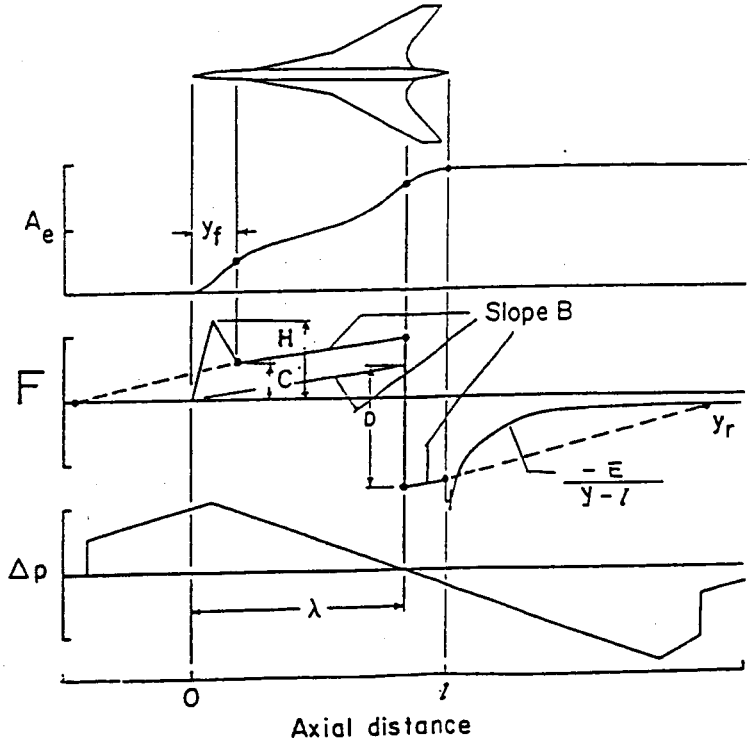

Figure 7. The *F*-function is characterised by the nine parameters as shown. A typical relationship among the equivalent area distribution, *F*-function, and pressure signal is described.

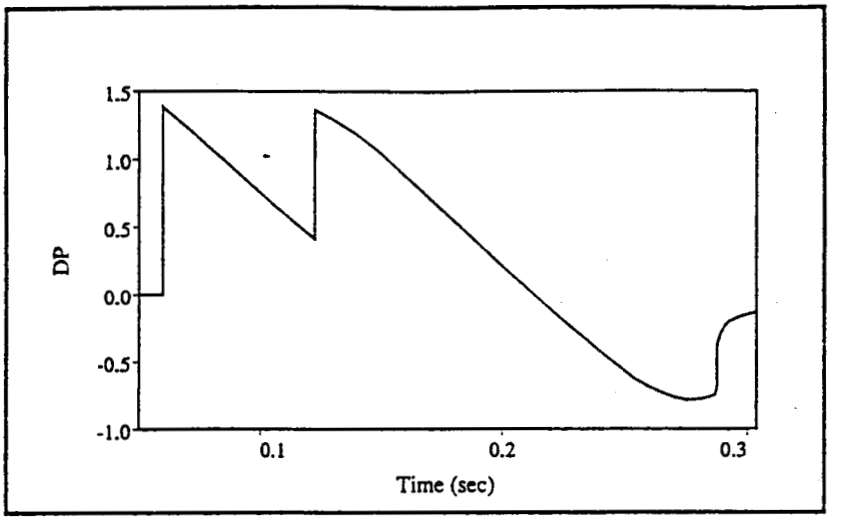

Figure 8. Sonic boom shape on the ground produced by the original configuration.

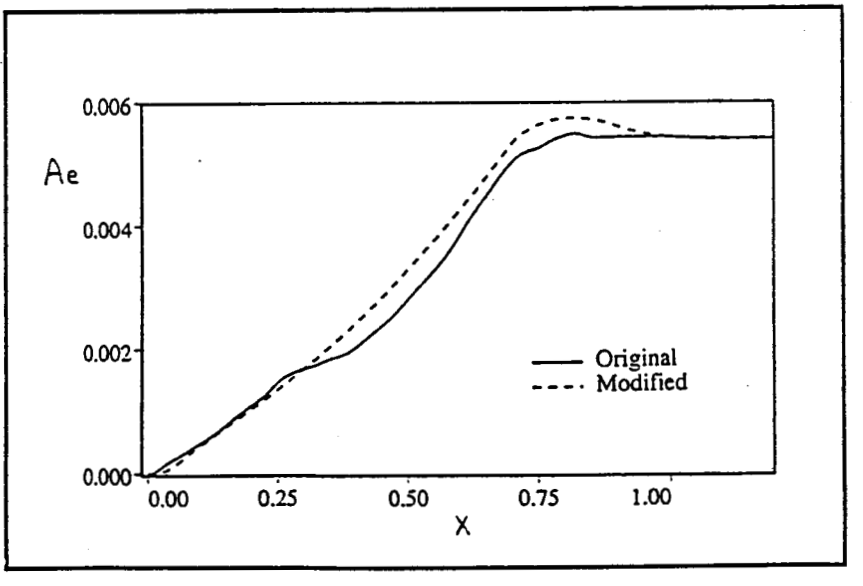

Figure 9. The difference in the equivalent area distributions between the original and the modified designs.

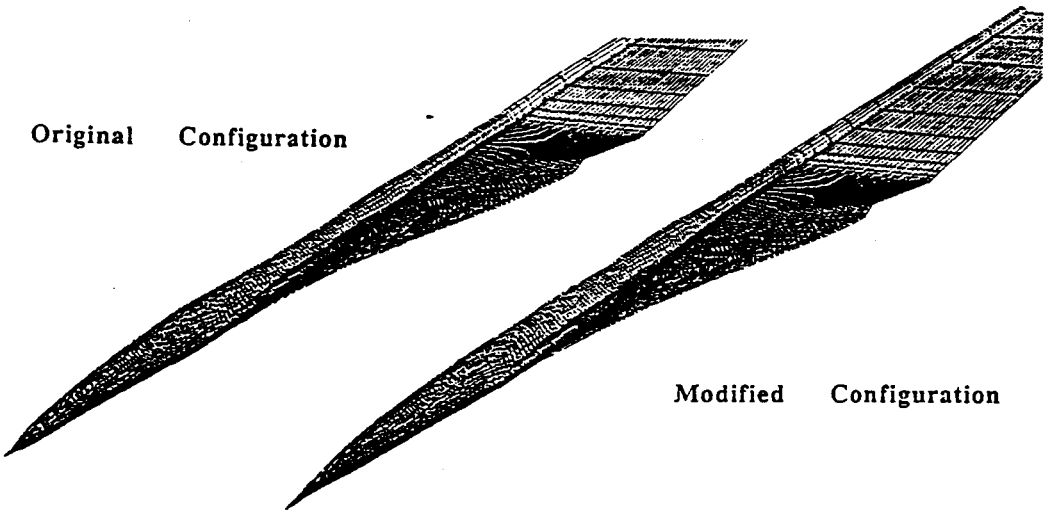

Figure 10. Comparison in the original and the modified configurations.

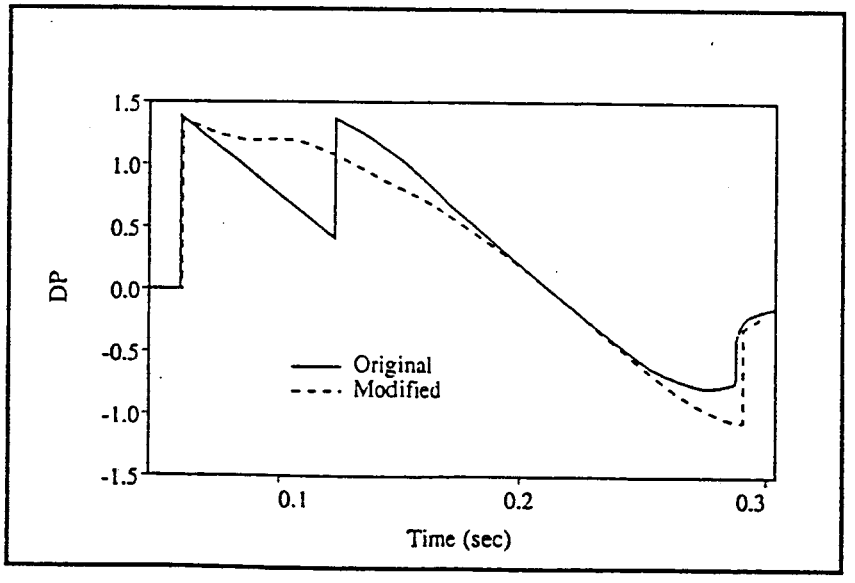

Figure 11. Comparison in the original and the modified sonic booms.